High-pressure phase equilibrium and volumetric properties of pseudo-binary mixtures of stock tank oil + methane up to 463K

Liu, Yiqun; Regueira, Teresa; Stenby, Erling Ha.; Yan, Wei

Published in:
Fluid Phase Equilibria

Link to article, DOI:
10.1016/j.fluid.2021.113054

Publication date:
2021

Document Version
Peer reviewed version

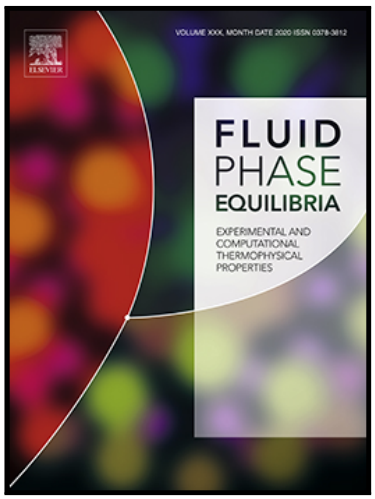

High-pressure phase equilibrium and volumetric properties of pseudo-binary mixtures of stock tank oil+methane up to 463K

Yiqun Liu , Teresa Regueira , Erling H. Stenby , Wei Yan

PII: S0378-3812(21)00116-3
DOI: https://doi.org/10.1016/j.fluid.2021.113054
Reference: FLUID 113054

To appear in: *Fluid Phase Equilibria*

Received date: 10 January 2021
Revised date: 21 March 2021
Accepted date: 7 April 2021

Please cite this article as: Yiqun Liu , Teresa Regueira , Erling H. Stenby , Wei Yan , High-pressure phase equilibrium and volumetric properties of pseudo-binary mixtures of stock tank oil+methane up to 463K, *Fluid Phase Equilibria* (2021), doi: https://doi.org/10.1016/j.fluid.2021.113054

High-pressure phase equilibrium and volumetric properties of pseudo-binary mixtures of stock tank oil + methane up to 463K

Yiqun Liu, Teresa Regueira, Erling H. Stenby, Wei Yan*

Center for Energy Resources Engineering (CERE), Department of Chemistry, Technical University of Denmark, DK-2800, Kgs. Lyngby, Denmark

* Email: weya@kemi.dtu.dk

Abstract

High-pressure phase equilibrium and volumetric properties of highly asymmetric mixtures related to reservoir fluids are critical to the development of high-pressure and high-temperature (HPHT) reservoirs. However, there is a lack of the relevant data and accurate modeling tools. In this work, we prepared asymmetric pseudo-binary mixtures of methane (CH_4) + stock tank oil (STO) and systematically measured their phase equilibrium and densities at temperatures from (298.15 to 463.15) K and pressures up to 140 MPa. The methane mole fraction in these mixtures range from 0.20 to 0.61 for the density measurement, and from 0.20 to 0.81 for the phase equilibrium measurement. From the experimental densities, the isothermal compressibility values, as well as the pseudo-excess volumes, were determined. Moreover, phase envelopes, relative volumes, and liquid volume fractions below the saturation point were also measured. These data are valuable for evaluating and improving thermodynamic models for HPHT reservoir fluids. The experimental results were modeled by the Soave-Redlich-Kwong (SRK) equation of state (EoS), the Peng-Robinson (PR) equation of state, their volume translated versions SRK-VT and PR-VT, and the Perturbed Chain Statistical Associating Fluid Theory (PC-SAFT). For density, SRK and PR gave large deviations of ~18% and ~8%, respectively, as compared with ~3% for PC-SAFT. Inclusion of volume translation reduced their deviations to the same level as that for PC-SAFT. For isothermal compressibility, all the models gave deviations of 20-30%, with PC-SAFT, SRK-VT and PR-VT being slightly better. The excess volumes calculated by SRK, PR and PC-SAFT were similar and close to the experimental values. The deviations in the calculated excess volumes resulted in only ~1% deviations in the calculated densities if the experimentally determined STO densities were used. It was illustrated that the small deviations could be utilized in the excess volume method to accurately estimate the high-pressure live oil densities from the high-pressure STO densities. This excess volume method gave ~1% density deviation on average for all the models, with PC-SAFT giving the smallest maximum deviation. The deviations in calculated saturation pressures were ~5% for all the models with the overall deviation for PC-SAFT being slightly smaller.

Keywords: Density, Phase equilibrium, High-pressure, Reservoir fluid, Asymmetric systems

1. Introduction

The global energy demand is expected to keep rising in the near future.[1] Although the fast-growing sustainable energy sector plays an increasingly important role in the total supply, the classical energy sources like oil and gas will still account for a significant portion in the coming decades.[1] Meanwhile, the conventional oil and gas resources are declining, pushing the oil industry to explore new frontiers like unconventional resources, such as shale,[2] or reservoirs at extreme conditions, such as high-pressure high-temperature (HPHT) reservoirs.[3][4]

The development of petroleum reservoirs needs an accurate description of the fluid phase behavior,[5]-[7] which provides fundamental information for determining the type of reservoir fluid, estimating the oil and gas in-place, and simulating the properties and composition of the fluid phases during production. These topics have been studied for decades but many challenges still exist, especially for HPHT reservoirs.[3] The challenges are rooted in the nature of reservoir fluids, most of which can be classified as asymmetric mixtures containing components with large contrast in molecular size and property. The high asymmetry of reservoir fluids can result in large and difficult to predict phase envelopes for gas condensate and volatile oil, and formation of additional liquid or solid hydrocarbon phases, such as wax and asphaltene precipitation.[7] Even for simple volumetric properties, like density and compressibility, accurate modeling of these asymmetric fluids over a wide temperature and pressure range, including HPHT conditions, is still unresolved, and there has always been an interest in improving the description using either classical models or more advanced ones.[8]-[11]

This study concerns the high-pressure volumetric and phase behavior of asymmetric mixtures related to reservoir fluids. There is no rigorous definition for these asymmetric mixtures but in general they contain light gas components, such as methane, nitrogen, and carbon dioxide, and much heavier hydrocarbons. For high-pressure fluid phase equilibria, there are extensive reviews [12]-[17] on the experimental methods and the systems investigated. Databases, such as [18] and [19], have an extensive collection of the vapor-liquid equilibrium data for hydrocarbon systems related to reservoir fluids. For high-pressure density data, several recent modeling studies[20]-[23] provide a relatively thorough summary of the data sources. However, it should be noted that the HPHT conditions[3] in the oil industry refer to pressures higher than 69 MPa and temperatures higher than 150 ^{o}C. Most of the high-pressure equilibrium and density data in the aforementioned sources do not belong to the HPHT conditions, therefore not directly useful. Some recent experimental efforts,[11],[24]-[34] including the measurements by our

laboratory,[30]-[34] have been dedicated to hydrocarbon systems at conditions more relevant to HPHT reservoirs. Most of these measurements are for well-defined binary mixtures. Gozalpour et al.[25][26] measured the viscosity and density of a six-component synthetic gas condensate and the equilibrium and density data of a five-component synthetic gas condensate. Regueira et al.[32][33] measured the equilibrium and volumetric data of four synthetic alkane mixtures, including two ternaries, one six-component gas condensate, and one six-component volatile oil. Only two of these recent studies use real reservoir fluids[34] or recombined fluids from crude oil[11]. The HPHT data for well-defined mixtures are still scarce, and it is always desirable to fill the gap with more measurements to assist the model development for these mixtures related to HPHT reservoir fluids. It should also be realized that the well-defined mixtures are not sufficiently representative of reservoir fluids, as shown by our previous studies.[30]-[34] This is because the heavy components in reservoir fluids are diverse and unique, and cannot be easily replaced by a few well-defined components.[32]-[34] For better modeling of real HPHT fluids, it is necessary to extend the measurement to real reservoir fluids or "synthetic" reservoir fluids containing the heavy ends from real reservoir fluids. Since it is costly to obtain real reservoir fluid samples, HPHT measurements of real reservoir fluids are rarely reported in the open literature. In comparison, it is easier to prepare live fluid mixtures using stock tank oil (STO) and light gas. An additional advantage of using STO is that the prepared mixtures can cover a range of gas-oil ratios. In fact, the two live oil samples measured by Burgess et al.[11] were prepared by combining two dead crude oils with methane. In this study, we prepared live fluid mixtures by combining methane and STO at different ratios, which is in contrast with our previous studies using well-defined mixtures[30]-[33] and real reservoir fluids.[34] These mixtures can be considered as pseudo-binaries of asymmetric components, and are better than the well-defined mixtures to represent real reservoir fluids.

We present below both the experimental measurement of the CH_4 + STO system and modeling of the measured data. The studied mixtures cover a broad composition range. Their high pressure densities were measured in the temperature range from (298.15 to 463.15) K and pressures up to 140 MPa, and their phase equilibrium were studied in the same temperature range. The values of the isothermal compressibility and the pseudo-excess volume were obtained from the measured densities. The measured phase equilibrium data include the phase envelopes, the relative volumes and the liquid fractions below the saturation point. Our measurement provides valuable data for evaluating and improving the models for HPHT reservoir fluids as well as for methane gas injection. The measured data were modeled by two cubic equations of state (EoSs), Soave-Redlich-Kwong (SRK) [35] and Peng-Robinson (PR) [36], and a non-cubic EoS Perturbed Chain Statistical Associating Fluid Theory (PC-SAFT).[37] The volume translated version of the cubic EoSs SRK-VT and PR-VT were also tested for property calculation. We also tested the recently proposed extend volume method[23] in the density modeling.

2. Materials and methods

2.1. Materials

n-Dodecane was used in the densimeter calibration and n-decane was used in the validation of the density measurement method. Both were purchased from Sigma-Aldrich with a mole fraction purity of 99%.

Methane was purchased from AGA GAS A/B with a mole fraction purity of 99.995%. We also used a stock tank oil (STO) obtained from a reservoir in the Danish sector of the North Sea. Prior to the experiments, the STO was centrifuged at 4000 rpm for 900 s to separate the water. The composition of the STO was determined up to the C_{24}^+ fraction by true boiling point (TBP) distillation through a TBP distillation unit FISCHER technology Labodest HMS 500 AC. The obtained composition, molecular weight and density for each fraction are presented in Table 1. The standard uncertainty for the reported mole fractions is estimated to be 0.002.

Table 1. Composition of the stock tank oil (STO) determined by true boiling point distillation.

Component	Mole fraction	Molar mass (g/mol)	Density at 15.6 °C (g/cm^3)
C_6	0.0966	85.52	0.6836
C_7	0.0732	100.84	0.7319
C_8	0.0928	109.19	0.7459
C_9	0.0815	125.21	0.7691
C_{10}	0.0576	138.27	0.7862
C_{11}	0.0493	147.12	0.7887
C_{12}	0.0549	160.88	0.7924
C_{13}	0.0731	167.40	0.7932
C_{14}	0.1228	183.03	0.7954
C_{15}	0.0484	198.67	0.8107
C_{16}	0.0292	213.20	0.8302
C_{17}	0.0248	229.08	0.8348
C_{18}	0.0211	244.92	0.8408
C_{19}	0.0094	251.33	0.8588
C_{20}	0.0146	256.80	0.8609
C_{21}	0.0167	267.12	0.8635
C_{22}	0.0076	284.35	0.8657
C_{23}	0.0114	290.21	0.8736
C_{24}^+	0.1150	426.92	0.9155

The density of the STO at 288.75 K and 0.1 MPa was determined through a densimeter Anton Paar DMA 4100. The measured value is 0.8082 g·cm^{-3}. The density of the C_7^+ fraction at 288.75 K and 0.1 MPa is 0.8151 g·cm^{-3}, as calculated from the densities measured for the STO and the C_6 fraction. The molecular weight obtained for the C_7^+ fraction is 197.39 g/mol.

In the pseudo-binary mixtures of CH_4 + STO, STO is considered to be a single component so that the pseudo-binaries consist of methane as component 1 and STO as component 2. The pseudo-binary mixtures used for the density measurement and for the phase equilibrium measurement were prepared separately.

In the density measurement, the pseudo-binary mixtures were prepared in a high-pressure sample cylinder with a floating piston, which separates the sample side from the hydraulic fluid side. The STO was added volumetrically to the sample side of the sample cylinder by using a burette (standard uncertainty 0.01 cm^3), afterwards methane was added gravimetrically by using an analytical balance Mettler-Toledo PR 1203 (standard uncertainty 0.001 g). The pressure in the sample cylinder was later increased with a syringe pump (Teledyne Isco 100 DX), which used water as hydraulic fluid and was connected to the hydraulic fluid side of the cylinder. The pressure of the injected sample was increased to a value higher than the saturation pressure to prepare a single-phase mixture. Rocking of the cylinder was performed to ensure that the single-phase sample was homogeneous. A new pseudo-binary mixture was prepared for each of the studied compositions. The mole fractions of CH_4 (x_1) in the prepared pseudo-binary mixtures CH_4 (1) + STO (2) are 0.2032, 0.4040, and 0.6133, respectively.

In the phase equilibrium measurement, the STO was first added volumetrically to the PVT cell by using a burette (standard uncertainty 0.01 cm^3). Subsequent successive additions of gas were performed gravimetrically by using the aforementioned analytical balance to achieve the desired compositions to be studied. The mole fractions of CH_4 (x_1) in the prepared pseudo-binary mixtures CH_4 (1) + STO (2) are 0.2046, 0.4039, 0.6007, 0.7033, and 0.8063 respectively.

2.2. Density measurement

The density measurement was performed in a high-pressure vibrating tube densitometer Anton Paar DMA HPM, in the temperature range from (298.15 to 463.15)K and pressures up to 140 MPa, by direct measurement of the oscillation period of a U-tube filled with the sample. The oscillating period was measured with 7 significant digits. A schematic of the experimental setup has been presented elsewhere. [31] The temperature control in the densimeter was performed through a circulating bath Julabo PRESTO A30 and measured by a temperature transducer Pt-100 located inside the cell close to the U-tube. The standard uncertainty of the temperature measurement is 0.02K. Pressure is generated by using a manual pressure generator HiP 37-6-30 and measured by means of a pressure transducer SIKA type P which measures pressures up to 150 MPa with a standard uncertainty of 0.05 % of the full scale.

The densimeter was calibrated in this work in the whole experimental temperature and pressure range following a modification of the method of Lagourette et al.,[38] as previously reported.[30][39]

Vacuum, Milli-Q water and n-dodecane were used as reference fluids for the calibration. In order to validate the calibration procedure of the densimeter, the density of n-decane was measured and compared with existing literature values. The obtained density values for n-decane are presented in Table S.1 in the supplementary information, whereas the relative deviations obtained after comparison with previously reported density values are depicted in Figure S.1 in the supplementary information. The relative deviations are within 0.3 % when compared with the data given by Lemmon and Span[40] and Cibulka and Hnědkovský.[41]

2.3. Isothermal compressibility and pseudo-excess volume

The experimental density data $\rho(T, p)$ were fitted to a modified Tammann-Tait equation,[42][43] given by the following equation:

$$\rho(T, p) = \frac{\rho(T, p_{ref})}{1 - C \ln\left[\frac{B(T) + p}{B(T) + p_{ref}}\right]} \tag{1}$$

where p_{ref} is a reference pressure and $\rho(T, p_{ref})$ is defined through the following polynomial equation:

$$\rho(T, p_{ref}) = \sum_{i=0}^{3} A_i T^i \tag{2}$$

C is a constant independent of temperature and pressure and $B(T)$ is a temperature dependent variable written as:

$$B(T) = \sum_{j=0}^{2} B_j T^j \tag{3}$$

Isothermal compressibility (κ_T) is a thermophysical property given by the following expression:

$$\kappa_T(T, p) = \frac{1}{\rho}\left(\frac{\partial \rho}{\partial p}\right)_T \tag{4}$$

In this work the isothermal compressibility values were obtained by differentiation from the Tammann-Tait fitting of the experimental density data as a function of temperature and pressure. The relative expanded isothermal compressibility uncertainty Ur(κ_T) (k=2) is 0.02.

We have defined the pseudo-excess volume (v^{PE}) of the studied pseudo-binary mixtures as follows:

$$v^{PE} = v - (x_G v_G + x_{STO} v_{STO}) \quad (5)$$

where x_G and x_{STO} are the mole fractions of the gas and the STO, respectively, and v_G and v_{STO} are the molar volumes of the methane and the stock tank oil, respectively. In the following discussion, we sometimes drop "pseudo" in the description for simplicity. The excess volumes in the pseudo-binary C1 + STO mixtures are always pseudo-excess volumes v^{PE} unless otherwise mentioned. To calculate v^{PE} from experimentally measured densities, we took methane molar volume from the NIST database and the STO molar volumes from the measured STO densities.

2.4. Phase equilibrium measurement

The phase equilibrium measurement was performed in a full visibility PVT cell from Sanchez Technologies. It consists of a variable volume cell with a piston in one end and a sapphire window in the other end. The piston is used to control the pressure in the cell, and it contains a set of retractable blades in its head used to stir the sample. There is a CCD digital camera Lumenera Lw1335C located in front of the sapphire window, which, together with the illumination of the cell by four optical fibers, allows the observation of the fluid inside the cell. The pressure in the cell is measured through a transducer Dynisco PT435A with a standard uncertainty of 0.06 MPa. Regarding temperature control, it is performed through a set of heating resistances located in the wall of the cell along with a thermostating liquid circulating in a jacket around the measuring cell, the temperature is measured through a Pt-100 located in the wall of the cell with a standard uncertainty of 0.02 K. The PVT cell has a rocking mechanism, which allows different positioning angles of the cell depending on the type of fluid to be studied. The system is fully controlled by means of the Falcon software. Saturation pressures and liquid fractions were determined by using this apparatus in the temperature range from (298 to 463) K. A schematic of the experimental setup has been previously reported.[32]

2.4.1. Saturation pressure and liquid fraction

The saturation pressure was determined by decreasing the pressure from the single-phase region with a flow rate of 5.6×10^{-4} $cm^3 \cdot s^{-1}$ until the appearance of a bubble/cloud was observed through the camera. The measurement was performed in triplicate. The combined standard uncertainty of the saturation pressure determination is estimated to be 0.1 MPa.

As concerns the liquid fraction below the saturation pressure, it was measured by using a constant mass expansion procedure (CME), in which the fluid was expanded in pressure steps in the single phase

region and subsequently in volume steps in the two phase region at constant temperature. In each step, the fluid was stirred for 300 s and successive waiting times of 600 s were applied until the pressure was stable within 0.05 MPa, at this moment the (*p*, *V*, *T*) conditions in the cell were recorded together with a photo of the fluid inside the cell. By using the Euclide software it was possible to analyze the photos in the two-phase region and measure the liquid volume for each step, which allowed determining the liquid fraction defined as V^{liq}/V^{tot}, where V^{liq} is the liquid volume and V^{tot} is the total volume of the system at given *p*, *T* conditions. Measurements of the relative volume V^{tot}/V^{sat}, where V^{sat} is the volume of the system at the saturation point, were also performed. The maximum standard liquid fraction uncertainty *u* (liquid fraction percentage) is 2.1 %.

2.5. Data modeling

The data measured in this work were modeled by using two cubic equations of state (EoSs), Soave-Redlich-Kwong (SRK)[35] and Peng-Robinson (PR) [36], and a non-cubic EoS, PC-SAFT[37].

2.5.1. SRK, PR and their volume-translated versions

The SRK and PR EoSs can be expressed in the following general form[44]

$$p = \frac{RT}{v-b} - \frac{a(T)}{(v+\delta_1 b)(v+\delta_2 b)} \tag{6}$$

where *R* is the universal gas constant, b is the covolume parameter, $a(T)$ is the energy parameter, and δ_1 and δ_2 are two model specific constants. For SRK, $\delta_1 = 1$ and $\delta_2 = 0$; for PR, $\delta_1 = 1+\sqrt{2}$ and $\delta_2 = 1-\sqrt{2}$. The parameters b and $a(T)$ in a mixture are calculated using the van der Waals one-fluid mixing rules:

$$b = \sum_i x_i b_i \tag{7}$$

$$a = \sum_i \sum_i x_i x_j \sqrt{a_i a_j}\,(1-k_{ij}) \tag{8}$$

where x_i is the mole fraction of the component *i* in the mixture. The expressions for the pure-component parameters b_i and a_i can be found in [35] [36] [44]. They need the pure-component critical temperatures T_{ci}, critical pressures P_{ci} and acentric parameters ω_i as input parameters. The binary interaction parameters

k_{ij} are usually determined by fitting binary equilibrium data. The k_{ij} values used in this study are taken from [10].

The two cubic models can be improved in their density calculation using the Peneloux volume translation.[45] The resulting models after volume translation are denoted by SRK-VT and PR-VT, respectively. The phase molar volumes v_{SRK} and v_{PR} from the original SRK and PR are corrected by the following volume translation equations, respectively:

$$v_{SRK-VT} = v_{SRK} - c_{SRK} \tag{9}$$

$$v_{PR-VT} = v_{PR} - c_{PR} \tag{10}$$

where v_{SRK-VT} and v_{PR-VT} are the molar volumes obtained after volume translation for SRK and PR, respectively; c_{SRK} and c_{PR} are the Peneloux volume translation parameters for SRK and PR, respectively. c_{SRK} and c_{PR} are calculated according to the following equation for a multicomponent mixture:

$$c = \sum_i x_i c_i \tag{11}$$

where c is the volume translation parameter (c_{SRK} or c_{PR}) for the mixture and c_i is the Peneloux volume correlation for the pure component i ($c_{SRK,i}$ or $c_{PR,i}$). For hydrocarbon components with a carbon number smaller than 7, the Peneloux volume corrections for SRK and PR are estimated according to the following equations[5]:

$$c_{SRK,i} = 0.40768 \frac{RT_{ci}}{P_{ci}} (0.29441 - Z_{RA,i}) \tag{12}$$

$$c_{PR,i} = 0.50033 \frac{RT_{ci}}{P_{ci}} (0.25969 - Z_{RA,i}) \tag{13}$$

$Z_{RA,i}$ is the Rackett compressibility factor[46] given by:

$$Z_{RA,i} = 0.29056 - 0.08775\omega_i \tag{14}$$

2.5.2. PC-SAFT

The PC-SAFT EoS is expressed in reduced Helmholtz energy $\tilde{a}$:

$$\tilde{a} \equiv \frac{A}{NkT} = \tilde{a}^{id} + \tilde{a}^{hc} + \tilde{a}^{disp} + \tilde{a}^{assoc} \tag{15}$$

where $\tilde{a}^{id}$ is the ideal gas contribution, $\tilde{a}^{hc}$ is the contribution of the hard-sphere chain reference system, $\tilde{a}^{disp}$ is the dispersion contribution arising from the square well attractive potential and $\tilde{a}^{assoc}$ is the association contribution based on Wertheim's theory. Here we used the simplified PC-SAFT proposed by von Solms et al.[47] instead of the original version. The simplified version has a form identical to Eq. (7) but slightly different mixing rules from those for the original version. Compared with the original version, the simplified PC-SAFT provides exactly the same results for pure components and very similar results for mixtures. The simplified version was chosen because it is more efficient in computation. A more detailed description of the original and the simplified PC-SAFT is provided in the supplementary information. For simplicity, we just use PC-SAFT in the following text when referring to the simplified version.

For systems without associating compounds, as in this study, the $\tilde{a}^{assoc}$ term disappears and there are just three model parameters for pure components: the segment length m_i, the segment diameter σ_i, and the energy parameter ε_i. For mixtures, there is one more interaction parameter k_{ij}. The parameters for well-defined pure components are taken from [37], and the k_{ij} parameters are from **Error! Reference source not found.**.

2.5.3. C_{7+} characterization

To calculate phase equilibrium and thermophysical properties for the STO and its mixtures with methane using an EoS, we need to characterize the ill-defined C_7^+ fraction in these systems. The purpose of C_7^+ characterization is to determine the detailed molar composition distribution usually in terms of single carbon number (SCN) components, to estimate EoS model parameters for the SCN components, and to come up with a manageable number of pseudo-components through lumping of the SCN components. The outcome from C_7^+ characterization is a list of pseudo-components with corresponding EoS model parameters, such as T_{ci}, P_{ci}, and ω_i for SRK and PR, and m_i, σ_i, and ε_i for PC-SAFT, which makes it possible to calculate the oil-containing system as an ordinary well-defined system.

For cubic EoSs, there are widely used characterization methods, such as the method of Pedersen et al.[48][49] and that of Whitson et al.[6][50] These methods can in principle be adapted to PC-SAFT by developing a set of correlations for the model parameters used in PC-SAFT, as described by Yan et al. [10] and Varzandeh et al. [52] Here we used the method of Yan et al. [10] for C_{7+} characterization. The method

uses the same procedure for calculation of the molar distribution in C_7^+ and the same lumping method as those in the method of Pedersen et al. [48][49], respectively. Consequently, the majority of the code for the method of Pedersen et al. can be directly reused and the characterization is easy to implement. For PC-SAFT, Yan et al. proposed a two-step perturbation method to estimate the PC-SAFT model parameters for a SCN component with known boiling point T_b and specific gravity SG. In the first step, the molecular weight of the n-alkane at this T_b, MW_0, can be estimated using Twu's correlations. [53] The PC-SAFT model parameters for n-alkanes, m_0, ε_0 and σ_0, are then calculated by the following linear correlations:

$$m_0 = 0.02644MW_0 + 0.83500 \tag{16}$$

$$m_0\varepsilon_0 / k = 6.90845MW_0 + 139.30870 \tag{17}$$

$$m_0\sigma_0^{\,3} = 1.71638MW_0 + 19.19189 \tag{18}$$

In the second step, the properties of the SCN component is estimated by using the difference in specific gravity $SG - SG_0$ as the perturbation parameter, where SG_0 is the specific gravity of the n-alkane calculated by Soave's correlation[54]:

$$SG_0 = \left(1.8T_b\right)^{1/3}\left(11.7372 + 3.336\times10^{-3}T_b - 976.3T_b^{-1} + 3.257\times10^{5}T_b^{-2}\right)^{-1} \tag{19}$$

The final PC-SAFT parameters for the SCN component are estimated by

$$\sigma = \sigma_0 \tag{20}$$

$$\varepsilon = \varepsilon_0(1.1303391\Delta SG + 1) \tag{21}$$

$$m = m_0(1.0460471\Delta SG^2 - 1.6209973\Delta SG + 1) \tag{22}$$

For SRK and PR, Yan et al. Suggested using a different set of correlations for the SRK and PR parameters from those used by Pedersen et al. Twu's correlations[53] are used for T_{ci} and P_{ci}, and the Lee-Kesler correlation[55][56] for ω_i. The SCN components above C_7 were finally lumped into 12 pseudo-components with nearly equal mass. The model parameters used for the pure and lumped components are presented in the supplementary information (Table S.2). It should be noted that the C_7^+ volume translation parameters for SRK and PR were obtained by matching the STO density at atmospheric pressure.

3. Results

We use the average absolute relative deviation (AARD) to compare the model results with the experimental data, which is defined as follows:

$$AARD/\% = \frac{100}{k}\sum_{i=1}^{k}\left|\frac{Y^{cal}-Y^{exp}}{Y^{exp}}\right| \tag{23}$$

where Y is the value of the studied property and k is the number of experimental data points. The superscripts *cal* and *exp* stand for calculated and experimental, respectively.

It is worth noting that in the case of the pseudo-excess molar volume (v^{PE}), a different deviation was used to compare the experimental results with the model calculations:

$$AARD^{*}/\% = \frac{100}{k}\sum_{i=1}^{k}\left|\frac{v^{PE,cal}-v^{PE,exp}}{v^{exp}}\right| \tag{24}$$

where v^{PE} is the pseudo-excess molar volume, v is the molar volume, and k is the number of data points. This deviation uses the experimental molar volume as the scaling parameter and represents the importance of the deviation in the predicted excess molar volume to the molar volume (or density).

3.1. Density

This section presents the high-pressure density data for STO and CH_4 + STO, and the comparison with model predictions.

3.1.1 Stock tank oil density

Table 2 presents the experimental density data of the STO. The measured densities show the typical trends with temperature and pressure, i.e., the density increasing with pressure along isotherms and decreasing with temperature along isobars. Density values at selected isotherms and isobars are plotted in Figure 1, together with the predictions obtained with the different models studied in this work.

Table 2. Experimental density (ρ) values of the STO in g·cm^{-3}

	T/K					
p/MPa	298.15	323.15	348.15	373.15	423.15	463.15
0.10	0.8021	0.7832	0.7646	0.7484	—	—
5.00	0.8033	0.7855	0.7674	0.7502	0.7122	0.6804
10.00	0.8062	0.7888	0.7713	0.7552	0.7189	0.6892
20.00	0.8103	0.7938	0.7771	0.7641	0.7304	0.7034

40.00	0.8173	0.8022	0.7868	0.7794	0.7493	0.7257
60.00	0.8277	0.8133	0.7989	0.7922	0.7646	0.7432
80.00	0.8373	0.8234	0.8098	0.8036	0.7777	0.7578
100.00	0.8459	0.8324	0.8194	0.8136	0.7894	0.7702
120.00	0.8540	0.8407	0.8282	0.8227	0.7995	0.7813
140.00	0.8615	0.8485	0.8364	0.8311	0.8087	0.7914

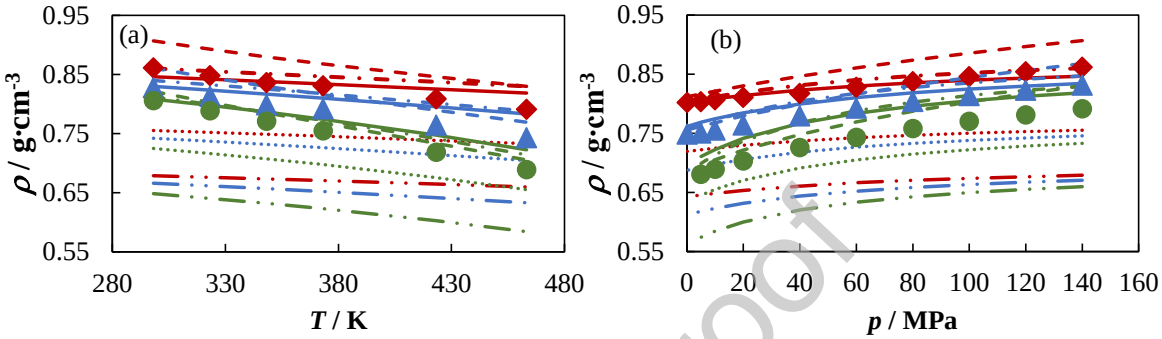

Figure 1. Experimental density data of the STO (a) as a function of temperature at (●) 10 MPa, (▲) 60 MPa and (◆) 140 MPa and (b) as a function of pressure at (◆) 298.15 K, (▲) 373.15 K and (●) 463.15 K. The lines represent the model predictions through (— • •) SRK, (•••) PR, (– –) PC-SAFT, (– •) SRK-VT and (—) PR-VT.

A quantitative evaluation of the model performance for the prediction of the STO density, through the analysis of the absolute average relative deviation, is presented in Figure 2, which shows both the performance at each temperature or pressure and the overall performance. The original SRK and PR gave very poor predictions, with SRK giving the maximum overall AARD (18%). SRK-VT and PR-VT have a similar performance to PC-SAFT. Actually, the two volume translated models are slightly better. It shows that volume translation is effective in improving the density calculation of SRK and PR. The similar density deviations from PC-SAFT and volume translated cubic EoSs were also observed in our previous study.[57]

It should also be noted that the PC-SAFT characterization, unlike those for SRK-VT and PR-VT, has not included the matching of the atmospheric STO density. Therefore, the PC-SAFT calculation is pure prediction. However, this is insufficient to explain the fact that PC-SAFT gives better agreement at low pressures and larger deviations at high pressures. It shows that the parameters obtained from the default PC-SAFT characterization should be improved.

The density deviations show some temperature and pressure dependence. Higher temperatures seem to favor the prediction of SRK and PR but the effect is just the opposite for SRK-VT and PR-VT. The PC-SAFT performance is not so affected by temperature, but the PC-SAFT prediction gets poorer at high pressures for this specific case. For SRK and PR, their predictions are closer at low pressures and the

deviations increase with pressure since the predicted density increase is insufficient. For SRK-VT and PR-VT, the pressure effect is not obvious.

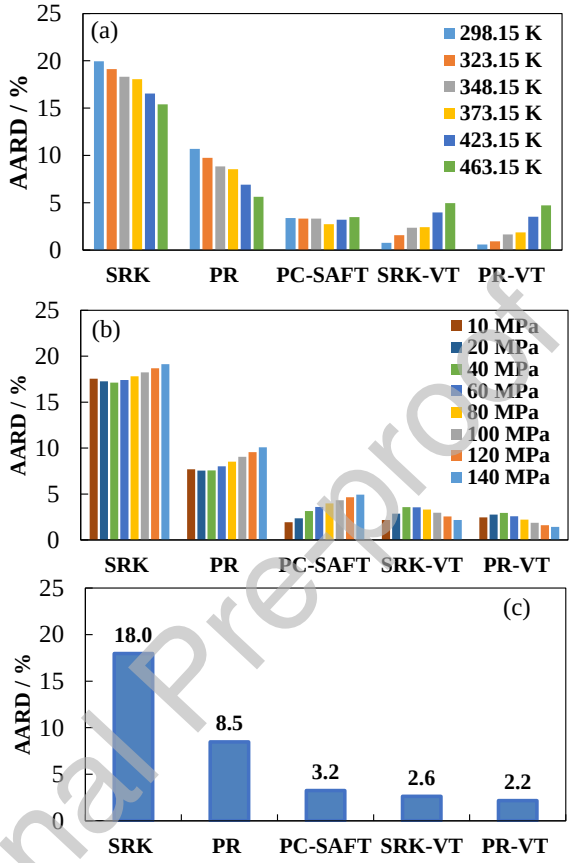

Figure 2. AARD (%) obtained in the prediction of the STO density through different models (a) as a function of temperature, (b) as a function of pressure and (c) overall deviation.

3.1.2 Density of the pseudo-binary CH_4+ STO mixtures

The experimental density values for the three different compositions studied are gathered in Table 3. Figure 3 shows the measured data at selected temperatures and pressures together with the results from the model predictions. Figure 5 summarizes the model performances for this pseudo-binary mixture. The figure shows that SRK-VT, PR-VT and PC-SAFT provide the best density prediction for these pseudo-binary mixtures. SRK-VT is the best among the three and PC-SAFT a bit inferior to the other two. The original SRK and PR yield the worst performance, and it shows again how volume translation can improve the performance of cubic models. All the models, except PR-VT, give better performance at a higher methane mole fraction. SRK and PR provide better predictions as the temperature increases, whereas no clear trend with temperature is observed for PC-SAFT and PR-VT, and the results for SRK-

VT get worse with increasing temperature. Finally, the predictions by SRK, PR and PC-SAFT get worse with increasing pressure whereas there is no significant pressure effect on SRK-VT and PR-VT.

It is interesting to note the similarity between the deviations reported in Figures 2 and 4, which indicates that the deviations in the density predictions of the STO have propagated to the predicted densities of the CH_4 + STO mixtures. This fact shows the importance of performing a good modeling of the STO density in order to obtain a satisfactory model of the live fluids that consist of mixtures of STO with dissolved gases.

Table 3. Experimental density values (ρ) for the pseudo-binary system CH_4 (1) + STO (2) in g·cm^{-3}.

	T/K					
p/MPa	298.15	323.15	348.15	373.15	423.15	463.15
	x_1=0.2032					
40.00	0.7907	0.7754	0.7587	0.7497	0.7173	0.6920
60.00	0.8019	0.7875	0.7720	0.7640	0.7345	0.7119
80.00	0.8121	0.7982	0.7837	0.7764	0.7489	0.7281
100.00	0.8213	0.8077	0.7940	0.7873	0.7615	0.7420
120.00	0.8297	0.8164	0.8034	0.7971	0.7725	0.7542
140.00	0.8374	0.8246	0.8121	0.8060	0.7824	0.7652
	x_1=0.4040					
40.00	0.7609	0.7446	0.7276	0.7180	0.6826	0.6558
60.00	0.7731	0.7582	0.7427	0.7342	0.7026	0.6791
80.00	0.7841	0.7700	0.7556	0.7480	0.7187	0.6975
100.00	0.7938	0.7803	0.7668	0.7598	0.7325	0.7129
120.00	0.8028	0.7897	0.7768	0.7703	0.7445	0.7261
140.00	0.8113	0.7984	0.7862	0.7798	0.7552	0.7378
	x_1=0.6133					
40.00	0.7051	0.6864	0.6670	0.6551	0.6172	0.5876
60.00	0.7202	0.7033	0.6860	0.6760	0.6431	0.6180
80.00	0.7330	0.7174	0.7015	0.6927	0.6627	0.6405
100.00	0.7440	0.7293	0.7146	0.7066	0.6791	0.6587
120.00	0.7539	0.7399	0.7261	0.7187	0.6928	0.6740
140.00	0.7628	0.7496	0.7365	0.7296	0.7051	0.6874

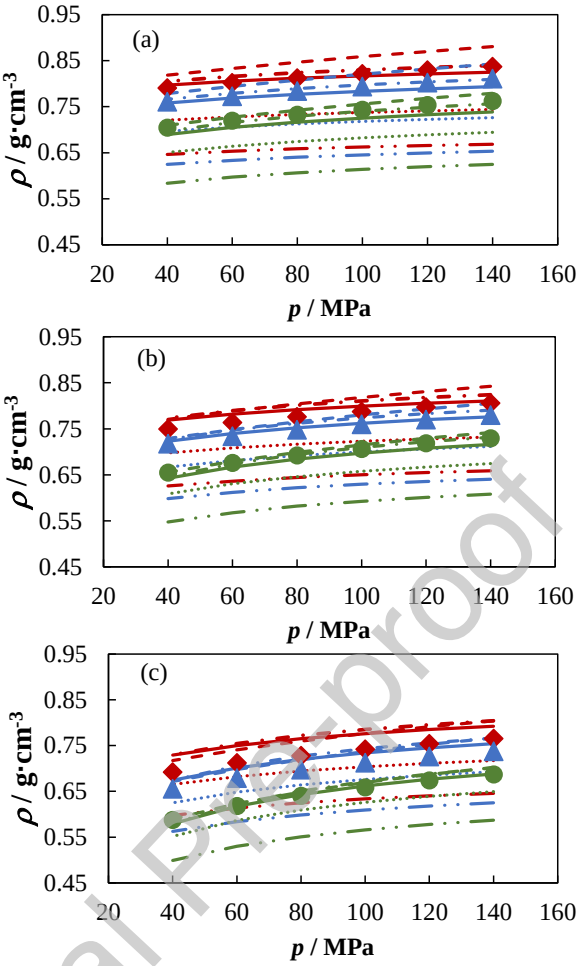

Figure 3. Experimental density data of the pseudo-binary system CH_4 (1) + STO (2) system as a function of pressure at (a) 298.15 K, (b) 373.15 K and (c) 463.15 K. (◆) x_1=0.2032, (▲) x_1=0.4040 and (●) x_1=0.6133. Lines represent model predictions through (— • •) SRK, (•••) PR, (– –) PC-SAFT, (– •) SRK-VT and (—) PR-VT.

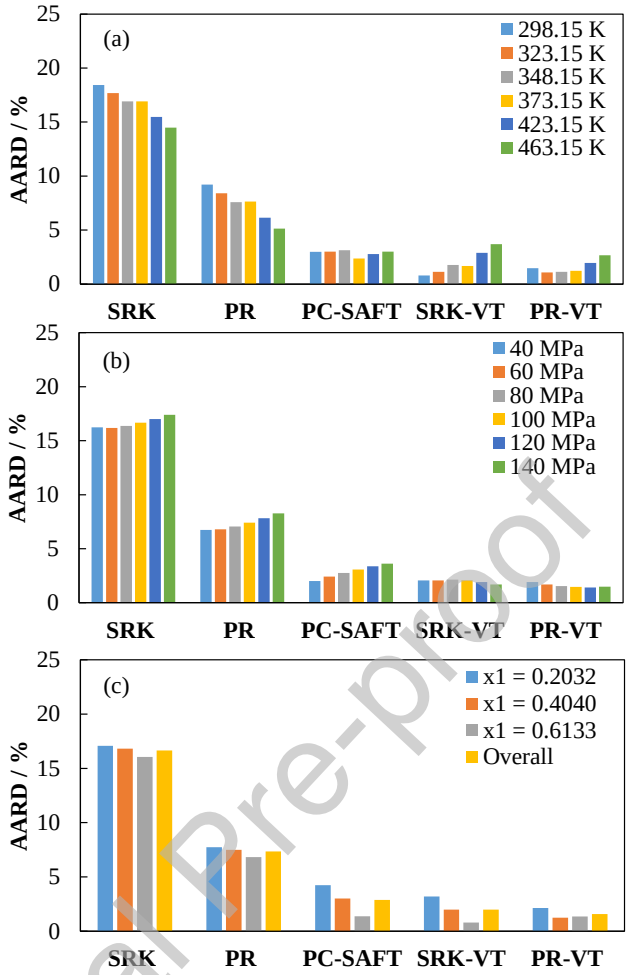

Figure 4. AARD (%) obtained in the prediction of the pseudo-binary system CH_4 (1) + STO (2) density through different models (a) as a function of temperature, (b) as a function of pressure and (c) as a function of composition and overall deviation.

3.2. Isothermal compressibility

The isothermal compressibility data were calculated using Eq. (4) by differentiating the density fitted to a modified Tammann-Tait equation (Eq. (1)). The coefficients of the Tammann-Tait fitting, together with the standard deviation of the fit, are gathered in Table 4.

The calculated compressibility data (κ_T) for STO and the C_1+STO mixtures are presented in Table 5. Figure 5 shows the compressibility data for the C_1+STO mixtures at selected temperatures along with the model predictions. As expected, the compressibility increases with temperature and methane mole fraction, but decreases with pressure.

Figure 6 presents the AARD in the predicted compressibility by different models. The deviations are high for all the models, and they decrease with increasing methane mole fraction. This is mainly because larger compressibility values at a higher methane mole fraction decreases the relative deviations.

The overall deviations in Figure 6 are all between 20% and 30% with that for PC-SAFT being slightly better. Figure 7 shows the average deviations only for the C_1+STO mixtures, i.e., excluding STO. The deviations are smaller than those in Figure 6 by 2%, again with the deviation for PC-SAFT being the smallest.

Table 4. Fitting parameters of the modified Tammann-Tait equation and AARD for the experimental density data of STO and the pseudo-binary system CH_4 (1) + STO (2)

	x_1=0.0000	x_1=0.2032	x_1=0.4040	x_1=0.6133
p_{ref} / MPa	5	40	40	40
A_0 /g·cm^{-3}	1.2384	1.2882	1.1815	1.1856
$10^3 \cdot A_1$ /g·cm^{-3}·K^{-1}	-2.6760	-3.3186	-2.6938	-3.0167
$10^6 A_2$ /g·cm^{-3}·K^{-2}	5.6843	7.6030	5.9811	6.4869
$10^9 A_3$ /g·cm^{-3}·K^{-3}	-5.4055	-6.9515	-5.6549	-5.9688
C	0.0973	0.0966	0.0968	0.10027
B_0 /MPa	561.87	258.59	242.56	247.13
B_1 / MPa·K^{-1}	-1.9735	-0.6778	-0.7006	-0.8842
$10^4 B_2$ / MPa·K^{-2}	18.134	3.4535	4.1028	7.1317
AARD/%	0.17	0.13	0.15	0.15

Table 5. Isothermal compressibility values ($10^3 \cdot \kappa_T$) for STO and the pseudo-binary system CH_4 (1) + STO (2) in MPa^{-1}.

	T/K					
p/MPa	298.15	323.15	348.15	373.15	423.15	463.15
			x_1=0.000			
10.00	0.67	0.79	0.93	1.11	1.60	2.10
20.00	0.64	0.74	0.86	1.01	1.39	1.76
40.00	0.57	0.65	0.74	0.85	1.12	1.35
60.00	0.52	0.58	0.66	0.74	0.93	1.09
80.00	0.47	0.53	0.59	0.66	0.81	0.92
100.00	0.44	0.48	0.53	0.59	0.71	0.80
120.00	0.41	0.45	0.49	0.54	0.64	0.71
140.00	0.38	0.41	0.45	0.49	0.58	0.64
			x_1=0.2032			
40.00	0.76	0.83	0.92	1.03	1.31	1.64
60.00	0.67	0.72	0.79	0.86	1.06	1.26
80.00	0.59	0.64	0.69	0.75	0.89	1.03
100.00	0.54	0.57	0.61	0.66	0.77	0.87
120.00	0.49	0.52	0.55	0.59	0.68	0.76
140.00	0.45	0.48	0.50	0.54	0.61	0.67
			x_1=0.4040			
40.00	0.87	1.01	1.18	1.37	1.79	2.11
60.00	0.73	0.83	0.94	1.05	1.29	1.44
80.00	0.63	0.70	0.78	0.85	1.00	1.09

100.00	0.58	0.61	0.66	0.72	0.82	0.88
120.00	0.52	0.54	0.58	0.62	0.70	0.74
140.00	0.48	0.48	0.51	0.55	0.60	0.64
			x_1=0.6133			
40.00	1.16	1.36	1.62	1.93	2.68	3.26
60.00	0.93	1.06	1.21	1.38	1.72	1.94
80.00	0.79	0.87	0.97	1.07	1.27	1.39
100.00	0.71	0.74	0.81	0.88	1.01	1.08
120.00	0.63	0.64	0.69	0.74	0.83	0.88
140.00	0.57	0.57	0.61	0.64	0.71	0.74

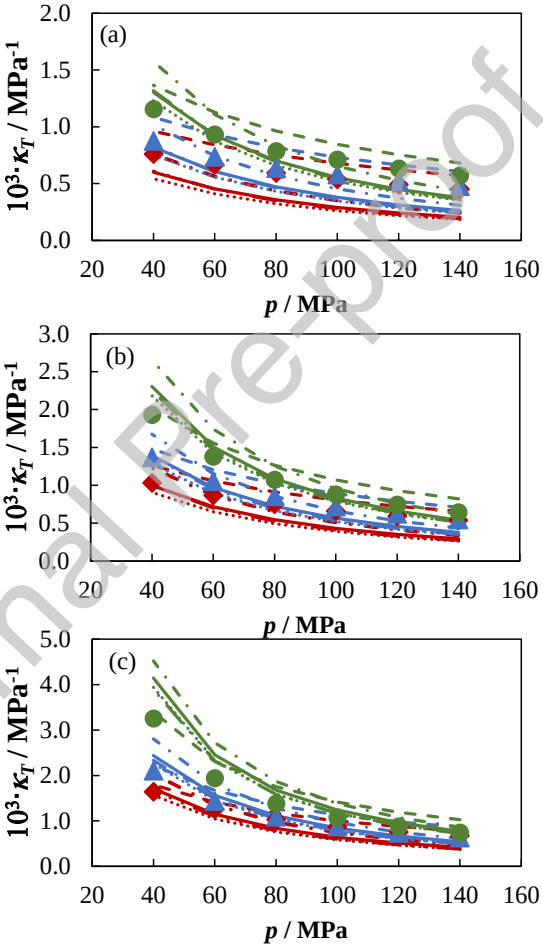

Figure 5. Isothermal compressibility (κ_T) data of the pseudo-binary system CH_4 (1) + STO (2) system as a function of pressure at (a) 298.15 K, (b) 373.15 K and (c) 463.15 K. (■) x_1=0.000, (◆) x_1=0.2032, (▲) x_1=0.4040 and (●) x_1=0.6133. Lines represent model predictions through (— • •) SRK, (•••) PR, (– –) PC-SAFT, (– •) SRK-VT and (—) PR-VT.

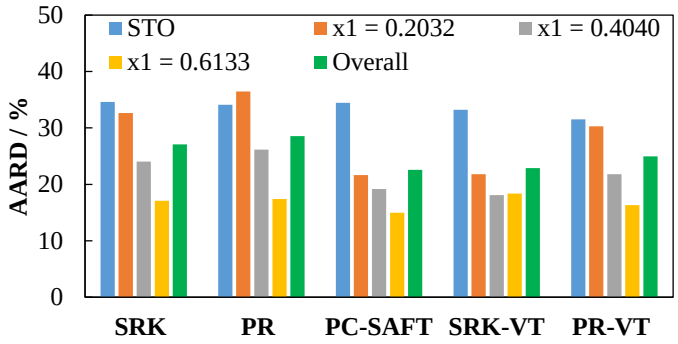

Figure 6. AARD (%) obtained in the prediction of the isothermal compressibility (κ_T) of STO and the pseudo-binary system CH_4 (1) + STO (2) through different models.

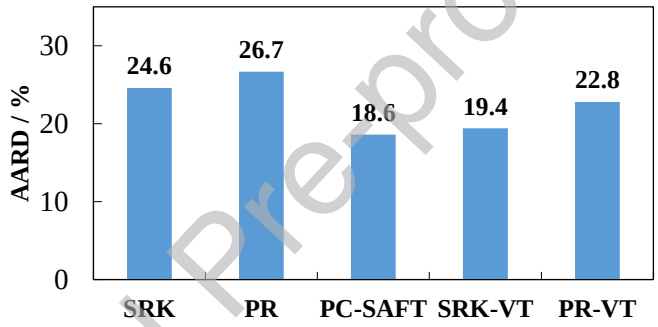

Figure 7. AARD (%) obtained in the prediction of the isothermal compressibility (κ_T) of the pseudo-binary system CH_4 (1) + STO (2) (excl. STO) through different models.

3.3. Pseudo-excess volume

Table 6 presents the pseudo-excess volumes determined from the measured densities. They are also shown in Figure 8 together with the prediction results from SRK, PR and PC-SAFT—the results from SRK-VT and PR-VT are not shown because volume translation does not change the calculated excess volume. The experimental pseudo-excess volumes are negative in most of the studied temperature and pressure conditions, indicating a volume reduction on mixing as compared to the ideal mixing. The pseudo-excess volume becomes more negative with increasing temperature, and less negative with increasing pressure. It approaches zero at the highest pressure 140 MPa, especially for the smallest methane mole fraction of 0.2. In the studied composition range (x_1=0.2 to 0.6), the pseudo-excess volume becomes more negative with increasing methane mole fraction. It is expected that the minima of these pseudo-excess volume curves are at higher methane fractions and these curves are asymmetric.

Table 6. Pseudo-excess volume (v^{PE}) for the pseudo-binary system CH_4 (1) + STO (2) in $cm^3 \cdot mol^{-1}$.

	T/K					
p/MPa	298.15	323.15	348.15	373.15	423.15	463.15
			x_1=0.2032			
40.00	-2.90	-3.78	-4.44	-5.19	-6.41	-7.23
60.00	-1.30	-1.76	-2.00	-2.32	-2.80	-3.19
80.00	-0.62	-0.94	-1.02	-1.17	-1.37	-1.54
100.00	-0.27	-0.46	-0.51	-0.61	-0.61	-0.84
120.00	-0.03	-0.18	-0.21	-0.28	-0.23	-0.42
140.00	0.12	-0.02	-0.02	-0.07	0.01	-0.18
			x_1=0.4040			
40.00	-7.51	-9.22	-10.9	-12.8	-15.4	-17.4
60.00	-4.29	-5.19	-5.99	-6.97	-8.18	-9.27
80.00	-2.91	-3.50	-3.99	-4.62	-5.22	-5.93
100.00	-2.13	-2.58	-2.93	-3.39	-3.67	-4.30
120.00	-1.66	-2.01	-2.27	-2.64	-2.80	-3.29
140.00	-1.38	-1.64	-1.88	-2.13	-2.23	-2.64
			x_1=0.6133			
40.00	-11.6	-14.0	-16.3	-19.0	-23.2	-26.1
60.00	-6.97	-8.07	-9.13	-10.6	-12.8	-14.4
80.00	-4.96	-5.65	-6.25	-7.21	-8.48	-9.58
100.00	-3.83	-4.31	-4.73	-5.43	-6.29	-7.14
120.00	-3.11	-3.49	-3.80	-4.36	-4.97	-5.67
140.00	-2.61	-2.94	-3.19	-3.66	-4.15	-4.73

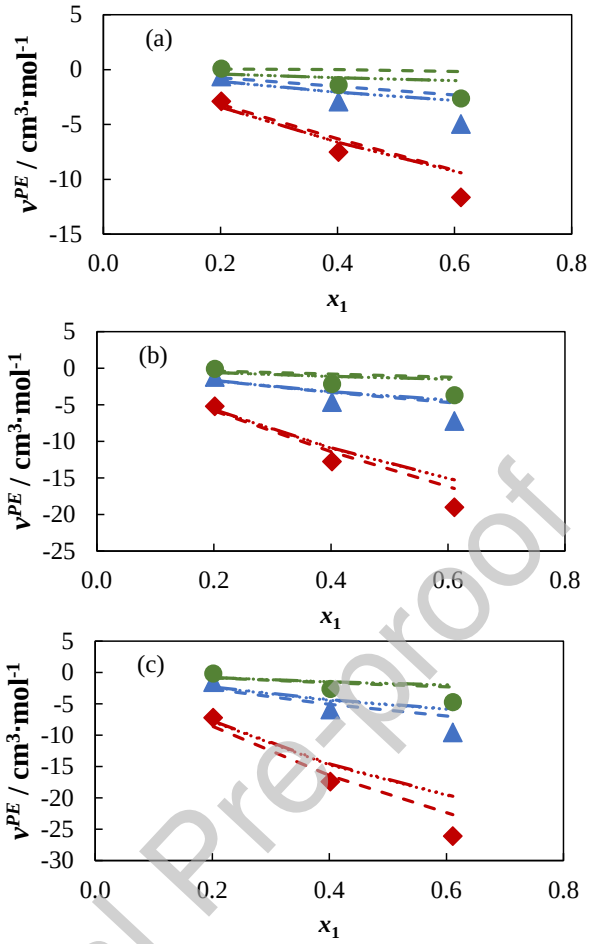

Figure 8. Pseudo-excess volume (v^{PE}) of the pseudo-binary system CH_4 (1) + STO (2) system as a function of pressure at (a) 298.15 K, (b) 373.15 K and (c) 463.15 K. (◆) 40 MPa, (▲) 80 MPa and (●) 140 MPa. Lines represent model predictions through (— • •) SRK, (•••) PR and (– –) PC-SAFT.

Figure 8 shows that SRK, PR and PC-SAFT predict similar excess volumes and they are all in decent agreement with the experimental data. We also observed that the similarity in calculated excess volumes in our previous experimental studies on high-pressure systems. [1-4] Figure 9 further presents the scaled deviations calculated using Eq. (12). These deviations reflect the importance of the prediction deviation in excess volume for the density value to be modeled. All three models give similar small deviations around 1%, which suggests that the differences in predicted densities are largely caused by the prediction deviations for the STO and methane densities. Another important implication is that since accurate methane densities are readily available and the STO densities can be accurately measured with a modest effort, the use of these data together with the excess volumes predicted by any of the three models (SRK, PR and PC-SAFT) should give close estimates for the actual densities.

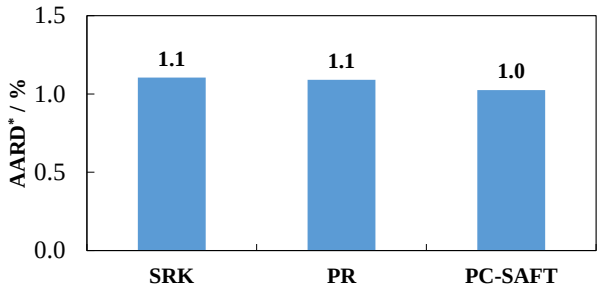

Figure 9. Average absolute deviations scaled by the experimental molar volume (AARD* /%) obtained in the prediction of the pseudo-excess volume of the pseudo-binary system CH_4 (1) + STO (2) through different models.

In our recent modeling study of high-pressure densities,[23] we also noted the similarity in excess volume between some cubic and non-cubic models, and proposed an excess volume method that calculate the molar volume from two different sources:

$$v = \sum x_i v_i^{p,II} + v^{E,I} \tag{25}$$

The pure-component molar volumes v_i^p are obtained from model II, which can be generally understood as a more accurate source for pure component densities. The excess volumes $v^{E,I}$ are obtained from an EoS model I, which can be a simple model or an easily accessible one. The method was tested against a large binary density database. For reservoir fluids, we proposed to use pseudo-excess volumes and calculate the reservoir fluid densities by

$$v = \sum_{i=1} x_i v_i^p + x_{STO}^G v_{STO}^G + v^{PE} \tag{26}$$

In the equation, STO is treated as one pseudo-component with its mole fraction x_{STO}^G and molar volume v_{STO}^G, the remaining components in the reservoir fluid are treated as individual components with mole fractions x_i and pure component molar volumes v_i^p, and v^{PE} is the pseudo-excess volume calculated by a model. For our CH_4+STO mixtures here, there is only one gas component methane. We tested the excess volume method with the pseudo-excess volumes calculated by different models. The experimental STO densities were used for the STO molar volumes but we calculated the methane density in two different ways:

- Excess volume method I: methane densities from the same model used for v^{PE}.
- Excess volume method II: methane densities from NIST

The overall deviations for all CH_4+STO mixtures are presented in Table 7 for the two excess volume methods and the original models. Two overall deviations are presented: the mean value of AARD and the

maximum of AARD (in parentheses). It can be seen that both excess volume methods have reduced the mean deviations to around 1%, and the reduction is especially significant for SRK and PR. For the excess volume method II, accurate NIST densities are used for methane and the deviations should in principle be smaller than those for the excess volume method I. However, the opposite is found for PR and PC-SAFT—PR with the excess volume method I actually gives the smallest deviation, which is due to cancellation of errors. SRK-VT and PR-VT are essentially the same as SRK and PR, respectively, when the method II is used. Therefore, they are not shown in Table 7 for the method II. In terms of maximum deviations, the excess volume methods generally show smaller values as compared with the respective original model except for SRK-VT and PR-VT. It should be noted that PC-SAFT gives a relatively stable performance in terms of the mean and maximum deviations. Here, we use the experimental STO densities directly. In a practical PVT modeling, it makes sense to tune EoS parameters to match STO densities for a better high-pressure density modeling.

Table 7. Overall deviations for calculated densities using different methods*

	SRK	PR	PC-SAFT	SRK-VT	PR-VT
Original models	16.65 (20.16)	7.35 (11.18)	2.88 (5.18)	1.99 (6.03)	1.58 (5.41)
Excess volume method I	1.10 (5.27)	0.64 (2.83)	0.83 (1.94)	0.95 (5.01)	1.23 (4.92)
Excess volume method II	1.08 (4.36)	1.07 (4.32)	1.01 (2.39)	-	-

* The deviations are the mean values of AARD (%) and the numbers in the parentheses are the maximum values.

3.4. Saturation pressure

The experimental values of the saturation pressure of the five pseudo-binary mixtures measured in this work are presented in Table 8 in the temperature range from (298 to 463) K. The values of the saturation pressure are depicted as a function of temperature for different isopleths in Figure 10. For lower methane mole fractions, p^{sat} increases with temperature, whereas the opposite trend is observed for the mixtures with higher methane mole fractions.

The increase of saturation pressure with methane mole fraction is presented in Figure 11 as a function of methane mole fraction at three selected temperatures, along with the model predictions obtained through SRK, PR and PC-SAFT. It can be observed that the models reproduce closely the experimental data, and similar results are obtained with the three models.

Figure 12 summarizes the model performance in terms of the overall AARDs and the deviations at different temperatures or different methane mole fractions. The overall AARDs obtained are very similar through the three models presented (around 5%), with PC-SAFT providing a slightly better performance. The predictions of saturation pressure with SRK and PR improve with increasing

temperature, and no obvious trend is found with methane mole fraction. Despite the fact that PC-SAFT prediction is slightly better for p^{sat} in the present work, it should be mentioned that in our previous works, [33]-[30],[57] we have found that a better performance of PC-SAFT compared to SRK and PR. It is worthwhile to note that the model performance of the saturation pressure prediction is case dependent. Moreover, there are even some cases where cubic EoSs provide a better representation of the saturation pressure.

Table 8. Saturation pressure (p^{sat}) for the pseudo-binary system CH_4 (1) + STO (2).

x_1=0.2046		x_1=0.4039		x_1=0.6007		x_1=0.7033		x_1=0.8063	
T/K	p^{sat}/MPa	T/K	p^{sat}/MPa	T/K	p^{sat}/MPa	T/K	p^{sat}/MPa	T/K	p^{sat}/MPa
298.15	4.46	298.17	11.75	298.12	25.95	298.11	39.27	298.27	56.42
323.15	5.08	323.11	13.07	323.14	27.24	323.03	39.19	323.33	53.60
348.17	5.61	348.14	14.08	348.21	28.11	348.13	39.10	348.12	51.80
373.17	6.05	373.19	14.86	373.18	28.64	373.02	38.83	373.20	50.19
423.21	6.75	423.22	15.81	423.16	28.85	423.16	37.72	423.09	46.86
463.10	7.18	463.21	16.10	463.15	28.43	463.18	36.05	463.24	44.09

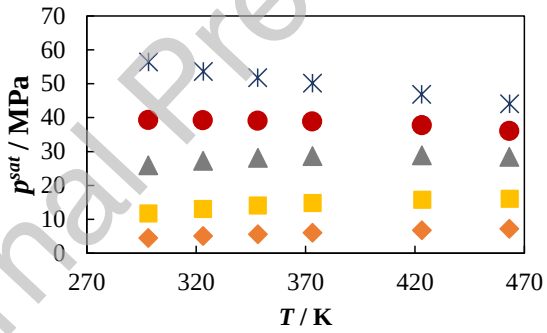

Figure 10. Saturation pressure (p^{sat}) of the pseudo-binary system CH_4 (1) + STO (2) as a function of temperature. (◆) x_1=0.2046, (■) x_1=0.4039, (▲) x_1=0.6007, (●) x_1=0.7033 and (∗) x_1=0.8063.

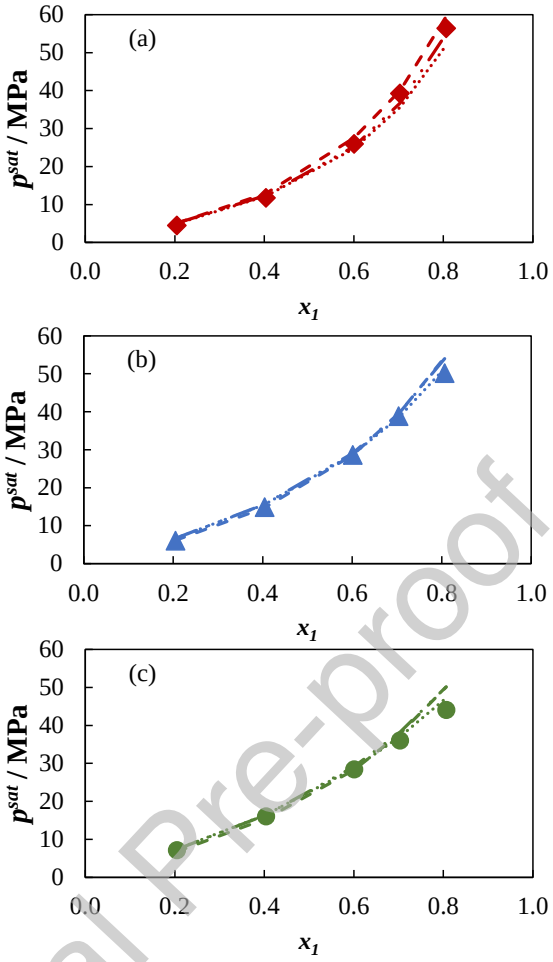

Figure 11. Saturation pressure (p^{sat}) of the pseudo-binary system CH_4 (1) + STO (2) as a function of methane mole fraction at (a) 298.15 K, (b) 373.15 K and (c) 463.15 K. Lines represent model predictions through (— • •) SRK, (•••) PR and (– –) PC-SAFT.

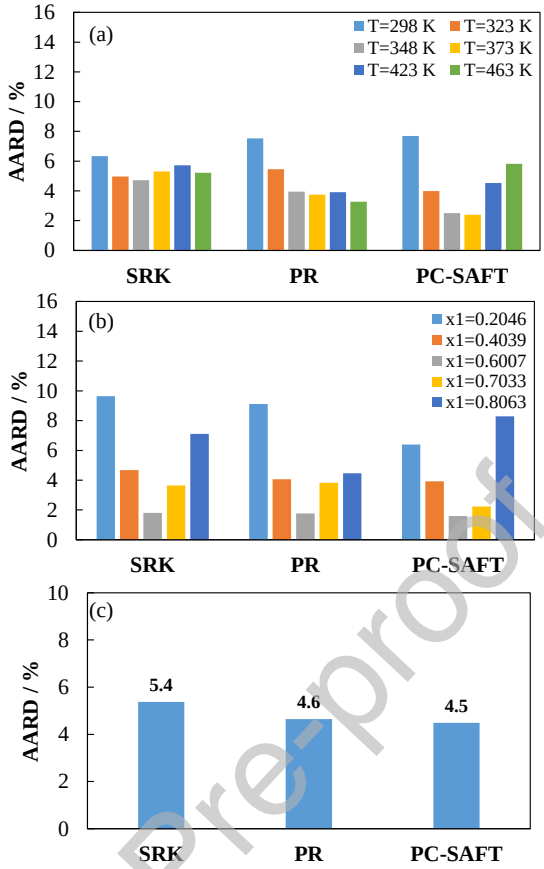

Figure 12. AARD (%) obtained in the prediction of the saturation pressure of the pseudo-binary system CH_4 (1) + STO (2) through different models (a) as a function of temperature, (b) as a function of CH_4 mole fraction (x_1) and (c) overall deviation.

3.5. Liquid fraction and relative volumes

Table 9 gathers the results of relative volume (V^{tot}/V^{sat}) and liquid fraction (V^{liq}/V^{tot}) from the constant mass expansion (CME). The relative volume is reported from a single phase state, corresponding to a relative volume value lower than 1, up to a maximum expansion between 2.5 and 4.3 times the saturation volume. This property is presented as a function of pressure in Figure 13 along with model predictions. It can be qualitatively observed that the three models SRK, PR and PC-SAFT provide good predictions of the relative volume in the studied pressure, temperature, and composition range.

The liquid fraction measured under expansion below the saturation point is plotted in Figure 14, a typical behavior of a bubble point system was obtained in the studied temperature, pressure and composition range. This means that the liquid fraction has a value of 1 at the saturation pressure and it decreases as the pressure decreases. It is interesting to remark that for the system with x_1=0.8048 at the temperatures of 373.15 K and 463.15 K the liquid fraction has a significant decrease right below the saturation pressure with a high slope of the V^{liq}/V^{tot} vs. p curve. This is an indication that the system is

approaching the critical point. The model predictions through SRK, PR and PC-SAFT are also presented in Figure 13, it is observed that the three models can capture the shape of the liquid fraction vs. pressure curves reasonably well, except for some poorer results by SRK and PR for x_1=0.8048. It is worth mentioning that the prediction results for the liquid fraction are affected by the saturation pressure predictions, as a value of 1 for the liquid fraction is achieved at the saturation pressure.

The quantitative evaluation of the model performance for relative volume and liquid fraction calculations is provided in Figure 15. It can be observed that the prediction of the relative volume is accomplished with an AARD lower than 3.5%, and the best prediction of this property is provided by PR. Regarding the liquid fraction, the best prediction is obtained by SRK with an AARD of 5.1%.

Table 9. Relative volume (V^{tot}/V^{sat}) and liquid fraction (V^{liq}/V^{tot}) for the pseudo-binary system CH_4 (1) + STO (2).

x_1=0.2046								
298 K			373 K			463 K		
p/MPa	V^{tot}/V^{sat}	V^{liq}/V^{tot}	p/MPa	V^{tot}/V^{sat}	V^{liq}/V^{tot}	p/MPa	V^{tot}/V^{sat}	V^{liq}/V^{tot}
20.41	0.979		22.35	0.971		11.96	0.981	
17.92	0.983		20.35	0.976		9.45	0.990	
16.07	0.985		18.41	0.978		9.46	0.990	
14.00	0.987		16.29	0.981		7.50	0.996	
11.70	0.988		14.40	0.983		7.31	0.997	
9.96	0.990		12.26	0.986		7.21	0.999	
8.18	0.992		10.43	0.989		7.18	1	1.000
6.29	0.995		8.37	0.993		7.15	1.005	0.933
4.46	1	1.000	6.34	0.998		6.98	1.018	0.836
4.39	1.005		6.05	1	1.000	6.66	1.044	0.696
4.37	1.008		5.98	1.007		6.12	1.096	0.513
4.34	1.014		5.79	1.021		5.12	1.226	0.382
4.21	1.029	0.990	5.46	1.050	0.974	3.92	1.487	
3.97	1.060	0.973	4.91	1.107	0.932	2.76	2.010	
3.54	1.122	0.935	3.95	1.252	0.834	1.99	2.794	
2.81	1.277	0.831	2.86	1.539	0.681	1.50	3.842	
1.98	1.588	0.683	1.88	2.118	0.513			
1.24	2.210	0.517	1.27	2.987	0.378			
0.77	3.143		0.90	4.146				
0.51	4.389							

x_1=0.4039								
298 K			373 K			463 K		
p/MPa	V^{tot}/V^{sat}	V^{liq}/V^{tot}	p/MPa	V^{tot}/V^{sat}	V^{liq}/V^{tot}	p/MPa	V^{tot}/V^{sat}	V^{liq}/V^{tot}
25.10	0.978		24.70	0.981		28.22	0.956	
23.68	0.982		22.95	0.985		25.91	0.965	
21.74	0.987		21.02	0.989		24.30	0.97	
19.57	0.990		18.92	0.992		22.22	0.977	
17.65	0.993		17.09	0.996		20.26	0.983	
15.58	0.995		14.86	1	1.000	18.23	0.991	
13.66	0.997		14.82	1.003		16.27	0.999	

11.75	1	1.000	14.62	1.008		16.10	1	1.000
11.68	1.003		14.13	1.021		16.09	1.001	
11.50	1.009		13.27	1.047		16.03	1.003	
11.01	1.023	0.986	11.89	1.099	0.917	15.88	1.008	
10.22	1.051	0.962	9.52	1.231	0.821	15.49	1.019	
9.01	1.107	0.915	6.91	1.497	0.650	14.78	1.043	
7.08	1.250	0.813	4.52	2.031	0.496	13.58	1.09	0.910
5.10	1.537	0.668	2.99	2.833		11.33	1.208	0.804
3.26	2.113	0.501	2.06	3.903		8.60	1.445	0.669
2.10	2.978					5.90	1.922	0.488
1.39	4.132					4.07	2.639	
						2.92	3.596	

x_1=0.6007

298 K			373 K			463 K		
p/MPa	V^{tot}/V^{sat}	V^{liq}/V^{tot}	p/MPa	V^{tot}/V^{sat}	V^{liq}/V^{tot}	p/MPa	V^{tot}/V^{sat}	V^{liq}/V^{tot}
35.95	0.986		36.45	0.981		38.27	0.956	
33.62	0.988		34.69	0.985		36.55	0.963	
31.95	0.990		32.80	0.989		34.58	0.970	
29.80	0.993		30.81	0.993		32.55	0.979	
27.85	0.995		28.85	0.998		30.56	0.989	
26.16	0.998		28.77	0.999		28.56	0.999	
26.06	0.999		28.64	1	1.000	28.43	1.000	1.000
25.95	1	1.000	28.55	1.001		28.22	1.002	
25.73	1.001		28.14	1.006		27.97	1.006	
25.04	1.006		27.21	1.017		27.37	1.016	
23.63	1.018		25.52	1.039	0.939	26.25	1.036	0.935
21.28	1.042		22.81	1.084	0.878	24.32	1.076	0.874
18.14	1.091	0.882	18.34	1.199	0.777	20.67	1.177	0.751
13.92	1.216	0.776	13.52	1.431	0.634	16.07	1.380	0.612
10.03	1.471	0.647	9.07	1.898	0.470	11.28	1.789	0.462
6.68	1.983	0.478	6.15	2.603		7.89	2.405	
4.50	2.754		4.31	3.543		5.67	3.227	
3.12	3.783							

x_1=0.7033

298 K			373 K			463 K		
p/MPa	V^{tot}/V^{sat}	V^{liq}/V^{tot}	p/MPa	V^{tot}/V^{sat}	V^{liq}/V^{tot}	p/MPa	V^{tot}/V^{sat}	V^{liq}/V^{tot}
49.55	0.982		49.25	0.971		46.38	0.949	
47.10	0.988		49.08	0.973		45.65	0.950	
45.29	0.990		47.06	0.978		44.12	0.956	
43.20	0.993		45.17	0.982		42.24	0.965	
41.30	0.996		43.10	0.987		40.26	0.975	
39.47	0.999		41.14	0.993		38.24	0.986	
39.27	1	1.000	39.16	0.999		36.27	0.999	
38.83	1.002		38.83	1.000	1.000	36.05	1.000	1.000
37.84	1.006		38.64	1.002		35.92	1.002	
35.52	1.015		38.15	1.005		35.65	1.005	
31.80	1.036	0.899	36.94	1.015		34.99	1.014	
26.63	1.078	0.828	34.79	1.034	0.898	33.78	1.031	0.867

19.87	1.189	0.723	31.29	1.074	0.827	31.63	1.065	0.787
14.22	1.415	0.605	25.41	1.174	0.714	27.39	1.151	0.670
9.65	1.873	0.457	18.99	1.378	0.591	21.84	1.325	0.548
6.67	2.561	0.334	13.03	1.790	0.450	15.78	1.676	0.418
4.74	3.481		9.02	2.410		11.27	2.205	
			6.43	3.240		8.22	2.912	

x_1=0.8063

298 K			373 K			463 K		
p/MPa	V^{tot}/V^{sat}	V^{liq}/V^{tot}	p/MPa	V^{tot}/V^{sat}	V^{liq}/V^{tot}	p/MPa	V^{tot}/V^{sat}	V^{liq}/V^{tot}
67.27	0.979		60.48	0.965		54.40	0.932	
66.45	0.981		60.32	0.966		54.13	0.933	
64.81	0.984		58.43	0.971		52.37	0.943	
62.73	0.988		56.43	0.977		50.39	0.954	
60.82	0.991		54.47	0.983		48.41	0.967	
58.82	0.995		52.51	0.990		46.40	0.981	
56.74	0.999		50.46	0.999		44.40	0.997	
56.62	0.999		50.33	0.999		44.26	0.998	
56.59	0.999		50.19	1	1.000	44.20	0.999	
56.42	1	1.000	50.06	1.001	0.945	44.16	0.999	
55.99	1.001		49.79	1.002	0.910	44.09	1	1.000
54.86	1.004		49.31	1.005	0.858	43.93	1.002	
52.17	1.012		48.10	1.013	0.794	43.70	1.004	0.603
47.71	1.028	0.759	45.83	1.028	0.730	43.15	1.011	0.584
40.57	1.061	0.699	42.05	1.059	0.662	42.00	1.024	0.563
30.03	1.149	0.625	35.22	1.138	0.585	39.98	1.050	0.533
21.06	1.330	0.533	27.26	1.299	0.492	35.79	1.116	0.486
14.43	1.700		19.44	1.623	0.391	29.84	1.249	0.419
10.29	2.258		13.94	2.114		22.69	1.518	0.336
7.56	3.003		10.23	2.770		16.89	1.922	
						12.68	2.463	

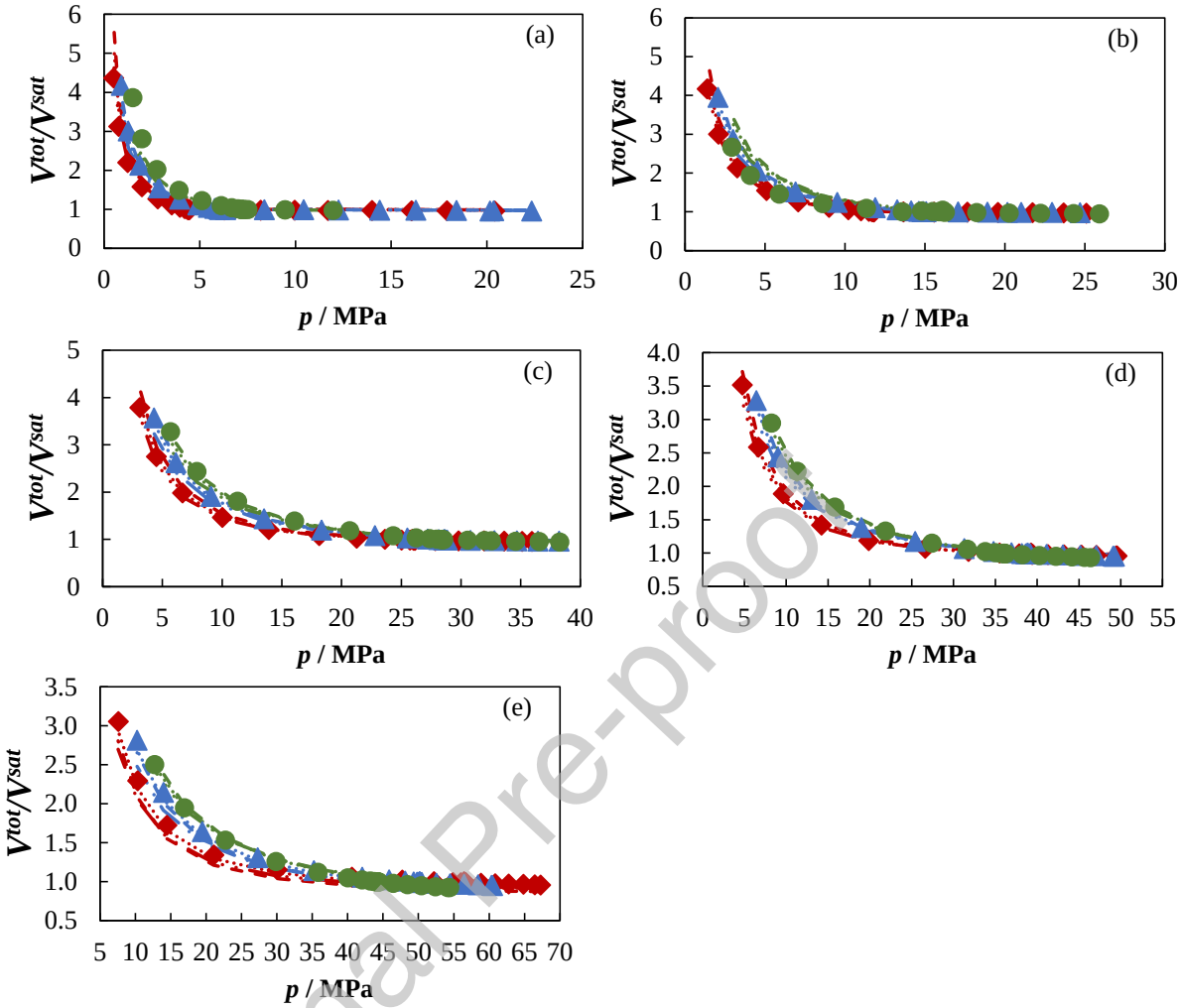

Figure 13. Experimental data of the relative volume of the pseudo-binary system CH_4 (1) + STO (2) as a function of pressure (a) x_1=0.2046, (b) x_1=0.4039, (c) x_1=0.6007, (d) x_1=0.7033 and (e) x_1=0.8063 at (◆) 298.15 K, (▲) 373.15 K and (●) 463.15 K. The lines represent the model predictions through (— • •) SRK, (•••) PR and (– –) PC-SAFT.

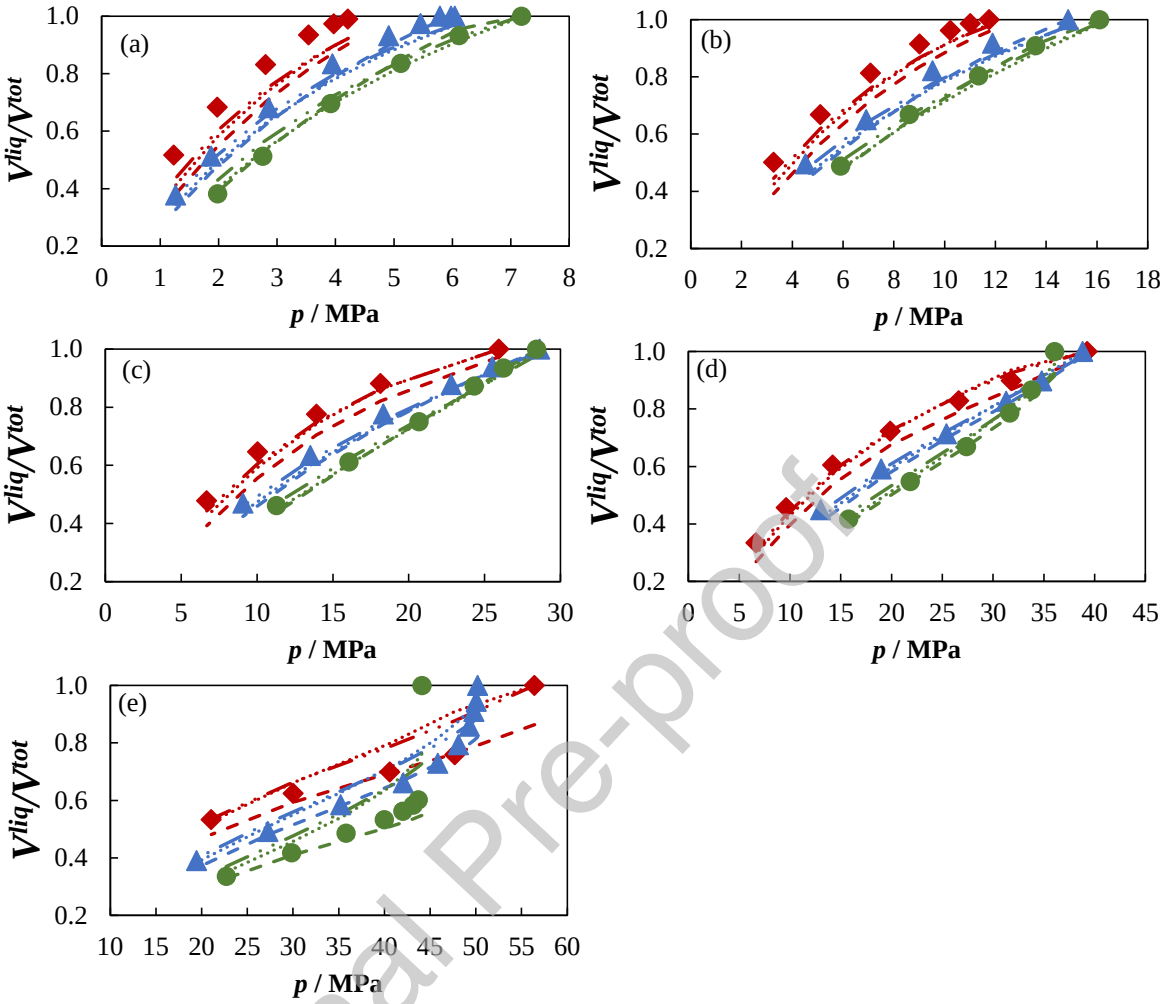

Figure 14. Experimental data of the liquid fraction of the pseudo-binary system CH_4 (1) + STO (2) as a function of pressure (a) x_1=0.2046, (b) x_1=0.4039, (c) x_1=0.6007, (d) x_1=0.7033 and (e) x_1=0.8063 at (◆) 298.15 K, (▲) 373.15 K and (●) 463.15 K. The lines represent the model predictions through (— • •) SRK, (•••) PR and (– –) PC-SAFT.

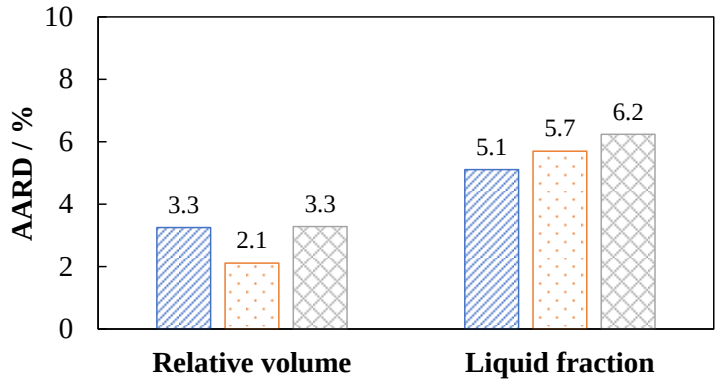

Figure 15. Average absolute relative deviations (AARD /%) obtained in the prediction of the relative volume and the liquid fraction of the pseudo-binary system CH_4 (1) + STO (2) through (diagonal striped) SRK, (dotted) PR, (crosshatched) PC-SAFT.

4. Conclusions

Real reservoir fluids contain ill-defined heavy ends that cannot be easily represented by a mixture of a few well-defined components. In order to better describe asymmetric reservoir fluid systems, we proposed to measure highly asymmetric mixtures prepared from STO and light gas in a systematic manner. We prepared CH_4 + STO mixtures in the methane mole fraction range from (0.20 to 0.61) for the density measurement, and (0.20 to 0.81) for the phase equilibrium measurement. In both types of measurement, the temperature range from (298.15 to 463.15) K and pressures up to 140 MPa are covered. The systematic measurement provided valuable high-pressure volumetric and phase equilibrium data for evaluating and improving thermodynamic models for HPHT reservoir fluids and for gas injection processes.

A comprehensive comparison was made using the measured data for SRK, PR, their volume translated versions SRK-VT and PR-VT, and PC-SAFT. It can be concluded that for density calculation, volume translation is essential for SRK and PR. The performance of PC-SAFT in density modeling is similar to that of PR-VT or SRK-VT for the measured mixtures although it is worthwhile to note that both the volume translation parameters in PR-VT and SRK-VT were tuned to match the C_{7+} density. It was found that the deviation in the predicted live oil density follows a similar trend to the deviation in the calculated STO density, showing the strong correlation between the live oil density and the STO density. For the isothermal compressibility of the measured mixtures, the performance of all the models are similar.

Pseudo-excess volume turns out to have a particular significance in modeling high-pressure densities. All the tested models gave similar pseudo-excess volumes, with deviations around 1% of the

total volume. This indicates that we can use any of the tested models to calculate the pseudo-excess volumes and then combine them with the STO densities, either measured or accurately modeled, to estimate the HPHT densities of asymmetric reservoir fluids with a relatively high-accuracy. This was illustrated for the measured mixtures using the recently proposed excess volume method. This method can potentially reduce the amount of experimental work needed for the more demanding live oil density measurement. Another important implication is that the accurate modeling of the STO densities in the temperature and pressure range of interest is the key to the accurate density modeling of the reservoir fluids.

PC-SAFT predicted slightly better saturation pressures than SRK and PR for the measured mixtures in the wide composition and temperature range, but the relative volumes and liquid fractions by different models are similar. It has been long questioned whether an advanced model like PC-SAFT outperforms the classical SRK and PR models in modeling HPHT reservoir fluids. The CH_4 + STO data measured in this study and the comparison based on them help us to give a more general and fair evaluation. It should be noted that some of the observations, especially those related to saturation pressure calculation, can be quite case-dependent. It is desirable to extend the study to systems consisting of other gas components and STO with different properties.

Nomenclature

a	energy parameter for SRK or PR
$\tilde{a}$	reduced Helmholtz energy
A	Helmholtz energy in Eq. (15)
A_i	Coefficients in Eq. (2)
b	co-volume parameter for SRK or PR
B	constants in the Tammann-Tait equation Eq. (1)
B_i	coefficients in Eq. (3)
c	volume shift parameter for SRK or PR
C	constant in the Tammann-Tait equation Eq.(1)
k	Boltzmann constant
k_{ij}	interaction parameter
MW	molecular weight
N	number of molecules

p	pressure
P_c	critical pressure
R	gas constant
SG	specific gravity
T	temperature
T_b	normal boiling temperature
T_c	critical temperature
v	molar volume
v_i^p	pure component molar volume for component *i*
V	volume
x_i	mole fraction
Z_{RA}	Rackett compressibility factor
ε	energy parameter
δ_1, δ_2	constants in SRK and PR
κ_T	isothermal compressibility
m	segment length
ρ	density
σ	segment diameter
ω	acentric factor

Subscripts

0	reference properties for n-alkanes
PR	PR EoS
ref	reference
SRK	SRK EoS
STO	Stock Tank Oil
VT	Volume Translated

Superscripts

assoc	association
disp	dispersion
E	excess properties
exp	experimental value

G	group
hc	hard chain
id	ideal gas
I	method I
II	method II
liq	liquid
cal	calculated value
sat	saturation point
tot	total
PE	pseudo-excess properties

Abbreviations

AARD	Average Absolute Relative Deviation
EoS	Equation of State
G	Gas
HPHT	High-Pressure High-Temperature
PC-SAFT	Perturbed Chain Statistical Associating Fluid Theory
PR	Peng-Robinson
SCN	Single Carbon Number
SRK	Soave-Redlich-Kwong
STO	Stock Tank Oil
TBP	True Boiling Point
VT	Volume Translation

Credit_Author_Statement

Y.Q. Liu contributed to experimental measurement and modeling. T. Regueira contributed to measurement. W. Yan contributed to modeling. All the authors contributed to research design and manuscript writing.

Declaration of interests

The authors declare that they have no known competing financial interests or personal relationships that could have appeared to influence the work reported in this paper.

References

[1] IEA (2020), World Energy Outlook 2020, IEA, Paris https://www.iea.org/reports/world-energy-outlook-2020

[2] IEA, US shale oil prospects, 2010-2024, IEA, Paris https://www.iea.org/data-and-statistics/charts/us-shale-oil-prospects-2010-2024

[3] G. DeBruijn, C. Skeates, R. Greenaway, D. Harrison, M. Parris, S. James et al. High-pressure, high-temperature technologies, Oilfield Rev, 20(2008) 46-60.

[4] U.S. Department of the Interior Bureau of Ocean Energy Management. HPHT Production in the Gulf of Mexico, OCS Report BOEM 2020-060. New Orleans, August 2020.

[5] L.P. Dake, Fudamentals of reservoir engineering, Elsevier Science, Amsterdam, the Netherlands, 1978.

[6] C. H. Whitson, M.R. Brule, Phase behavior, SPE Monograph Series Vol. 20, Society of Petroleum Engineers, 2000.

[7] K.S. Pedersen, P.L. Christensen, Phase Behavior of Petroleum Reservoir Fluids, Taylor & Francis Group, New York, 2007.

[8] J. Larsen, H. Sørensen, T. Yang, K.S. Pedersen, EoS and viscosity modeling for highly undersaturated Gulf of Mexico reservoir fluids, SPE-147075-MS presented at the SPE Annual Technical Conference and Exhibition, October 30-November 2, 2011.

[9] H. Baled, R.M. Enick, Y. Wu, M.A. McHugh, W. Burgess, D. Tapriyal, B.D. Morreale, Prediction of hydrocarbon densities at extreme conditions using volume-translated SRK and PR equations of state fit to high temperature, high pressure PVT data, Fluid Phase Equilib. 317 (2012) 65–76.

[10] W. Yan, F. Varzandeh, E.H. Stenby, PVT modeling of reservoir fluids using PC-SAFT EoS and Soave-BWR EoS, Fluid Phase Equilib., 386 (2015) 96-124.

[11] W.A. Burgess, B.A. Bamgbade, I.K. Gamwo, Experimental and predictive PC-SAFT modeling results for density and isothermal compressibility for two crude oil samples at elevated temperatures and pressures, Fuel 218 (2018) 385-395.

[12] R. Fornari, P. Alessi, I. Kikic, High-pressure fluid phase-equilibria—Experimental methods and systems investigated (1978-1987), Fluid Phase Equilib. 57 (1990) 1-33.

[13] R. Dohrn, G. Brunner, High-pressure fluid-phase equilibria: Experimental methods and systems investigated (1988-1993), Fluid Phase Equilib. 106 (1995) 213-282.

[14] Christov, M., Dohrn, R., High-pressure fluid phase equilibria: Experimental methods and systems investigated (1994-1999), Fluid Phase Equilib. 202 (2002) 153-218.

[15] R. Dohrn, S. Peper, J. Fonseca, High-pressure fluid-phase equilibria: Experimental methods and systems investigated, Fluid Phase Equilib. 288 (2010) 1-54.

[16] J. Fonseca, R. Dohrn, S. Peper, High-pressure fluid-phase equilibria: Experimental methods and systems investigated (2005-2008), Fluid Phase Equilib. 300 (2011) 1-69.

[17] S. Peper, J. Fonseca, R. Dohrn, High-pressure fluid-phase equilibria: Trends, recent developments, and systems investigated (2009-2012), Fluid Phase Equilib. 484 (2019) 126-224.

[18] H. Knapp, R. Doring, L. Oellrich, U. Plocker, J.M. Prausnitz, Chemical data series, Vapor–Liquid Equilibria for Mixtures of Low Boiling Substances, vol. VI, DECHEMA, Frankfurt, 1982.

[19] A. Maczynski, A. Skrzecz, TRC Data Bases for Chemistry and Engineering Floppy Book on Vapor–Liquid Equilibrium Data. Binary Systems Version 1998-1, Thermodynamics Data Center, Institute of Physical Chemistry and Institute of Coal Chemistry of the Polish Academy of Sciences.

[20] J.F. Estela-Uribe, An improved Helmholtz energy model for non-polar fluids and their mixtures. Part 2: Application to mixtures of non-polar fluids, Fluid Phase Equilib. 354 (2013) 326–343.

[21] J.F. Estela-Uribe, An improved Helmholtz energy model for non-polar fluids and their mixtures. Part 3: Application to natural gases and related systems, Fluid Phase Equilib. 356 (2013) 229–345.

[22] A. Gonzalez Perez, C. Coquelet, P. Paricaud, A. Chapoy, Comparative study of vapour-liquid equilibrium and density modelling of mixtures related to carbon capture and storage with SRK, PR,

PC-SAFT and SAFT-VR Mie equations of state for industrial uses, Fluid Phase Equilib. 427 (2016) 371-383.
[23] W. Yan, T. Regueira, Y. Liu, E.H. Stenby, Density modeling of high-pressure mixtures using cubic and non-cubic EoS and an excess volume method, Fluid Phase Equilib. 532 (2021) 112884.
[24] B. Tohidi, A.C. Todd, A. Danesh, R.W. Burgess, and F. Gozalpour, Viscosity and density of methane+cis-decalin from 323 to 424 K at pressures to 140 MPa, Int. J. Thermophysics 22(2001) 1661-1668.
[25] F. Gozalpour, A. Danesh, A.C. Todd, B. Tohidi, Viscosity and density data for a six-component model fluid at temperatures to 423 K and pressures to 140 MPa, High Temperatus-High Pressures 34 (2002) 483-486.
[26] F. Gozalpour, A. Danesh, A.C. Todd, D.H. Tehrani, B. Tohidi, Vapour-liquid equilibrium volume and density measurements of a five-component gas condensate at 278.15-383.15 K, Fluid Phase Equilib. 206 (2003) 95-104.
[27] F. Gozalpour, A. Danesh, A.C. Todd, B. Tohidi, Experimental data on binary and ternary mixtures of perfluoromethylcyclohexane with methane and n-decane at 373.15 K, J. Chem. Eng. Data 50 (2005) 1814-1817.
[28] B.A. Bamgbade, Y. Wu, W.A. Burgess, D. Tapriyal, I.K. Gamwo, H.O. Baled, R.M. Enick, M.A. McHugh, Measurements and modeling of high-temperature, high-pressure density for binary mixtures of propane with n-decane and propane with n-eicosane, J. Chem. Thermodynamics 84 (2015) 108-117.
[29] B.A. Bamgbade, Y. Wu, W.A. Burgess, D. Tapriyal, I.K. Gamwo, H.O. Baled, R.M. Enick, M.A. McHugh, High-temperature, high-pressure volumetric properties of propane, squalane, and their mixtures: Measurement and PC-SAFT modeling, Ind. & Eng. Chem. Res. 54 (2015) 6804-6811
[30] T. Regueira, W. Yan, E.H. Stenby, Densities of the binary systems n-hexane + n-decane and n-hexane + n-hexadecane up to 60 MPa and 463 K, J. Chem. Eng. Data, 60 (2015) 3631-3645.
[31] T. Regueira, G. Pantelide, W. Yan, E.H. Stenby, Density and phase equilibrium of the binary system methane + n-decane under high temperatures and pressures, Fluid Phase Equilib., 428 (2016) 48-61.
[32] T. Regueira, Y. Liu, A.A. Wibowo, M. Ashrafi, F. Varzandeh, G. Pantelide, E.H. Stenby, W. Yan, High pressure phase equilibrium of ternary and multicomponent alkane mixtures in the temperature range from (283 to 473) K, Fluid Phase Equilib., 449 (2017) 186-196.
[33] T. Regueira, M.-L. Glykioti, E.H. Stenby, W. Yan, Density and compressibility of multicomponent n-alkane mixtures up to 463 K and 140 MPa, J. Chem. Eng. Data, 63 (2018) 1072-1080.
[34] T. Regueira, M.-L. Glykioti, N. Kottaki, E.H. Stenby, W. Yan, Density, compressibility and phase equilibrium of high pressure-high temperature reservoir fluids up to 473 K and 140 MPa, J. of Supercritical Fluids 159 (2020) 104781.
[35] G. Soave, Equilibrium constants from a modified Redlich-Kwong equation of state, Chem. Eng. Sci., 27 (1972) 1197-1203.
[36] D.-Y. Peng, D.B. Robinson, A new two-constant Equation of State, Ind. Eng. Chem. Fundam., 15 (1976) 59-64.
[37] J. Gross, G. Sadowski, Perturbed-Chain SAFT: An equation of state based on a perturbation theory for chain molecules, Ind. Eng. Chem. Res., 40 (2001) 1244-1260.
[38] B. Lagourette, C. Boned, H. Saint-Guirons, P. Xans, H. Zhou, Densimeter calibration method versus temperature and pressure, Meas. Sci. Technol., 3 (1992) 699-703.
[39] M.J.P. Comuñas, J.-P. Bazile, A. Baylaucq, C. Boned, Density of diethyl adipate using a new vibrating tube densimeter from (293.15 to 403.15) K and up to 140 MPa. Calibration and measurements, J. Chem. Eng. Data, 53 (2008) 986-994.
[40] E.W. Lemmon, R. Span, Short fundamental equations of state for 20 industrial fluids, J. Chem. Eng. Data, 51 (2006) 785-850.

[41] I. Cibulka, L. Hnědkovský, Liquid densities at elevated pressures of n-alkanes from C5 to C16: A critical evaluation of experimental data, J. Chem. Eng. Data, 41 (1996) 657-668.
[42] J. Dymond, R. Malhotra, The Tait equation: 100 years on, Int. J. Thermophys., 9 (1988) 941–951.
[43] G. Tammann, The dependence of the volume of solutions on pressure, Z. Phys. Chem. Stoechiom. Verwandtschafts., 17 (1895) 620–636.
[44] M.L. Michelsen, J.M. Mollerup, Thermodynamic models: Fundamentals & computatioal aspects, 2nd ed., Tie-Line publications, 2007.
[45] A. Péneloux, E. Rauzy, R. Fréze, A consistent correction for Redlich-Kwong-Soave volumes, Fluid Phase Equilib., 8 (1982) 7-23.
[46] T. Yamada, R.D. Gunn, Saturated liquid molar volumes. Rackett equation, J. Chem. Eng. Data, 18 (1973) 234-236.
[47] N. von Solms, M.L. Michelsen, G.M. Kontogeorgis, Computational and physical performance of a modified PC-SAFT Equation of State for highly asymmetric and associating mixtures, Ind. Eng. Chem. Res., 42 (2003) 1098-1105.
[48] K.S. Pedersen, A. Fredenslund, P. Thomassen, Properties of oils and natural gases, Gulf Publishing Inc, Houston, 1989.
[49] K.S. Pedersen, P. Thomassen, A. Fredenslund, Characterization of gas condensate mixtures, in: L.G. Chorn, G.A. Mansoori (Eds.), Advances in Thermodynamics, Vol.1-C7+ Fraction Characterization, Taylor & Francis, New York, 1989, pp. 137-152..
[50] C.H. Whitson, T.F. Anderson, I. Søreide, in: L.G. Chorn and G.A. Mansoori (Eds.), Advances in Thermodynamics, Vol.1-C7+ Fraction Characterization, Taylor & Francis, New York, 1989, pp. 35-56.
[51] W. Yan, F. Varzandeh, E.H. Stenby, PVT modeling of reservoir fluids using PC-SAFT EoS and Soave-BWR EoS, Fluid Phase Equilib., 386 (2015) 96-124.
[52] F. Varzandeh, E.H. Stenby, W. Yan, General approach to characterizing reservoir fluids for EoS models using a large PVT database, Fluid Phase Equilib., 433 (2017) 97-111.
[53] C.H. Twu, An internally consistent correlation for predicting the critical properties and molecular weights of petroleum and coal-tar liquids, Fluid Phase Equilib., 16 (1984) 137-150.
[54] G. Soave, Estimation of the critical constants of heavy hydrocarbons for their treatment by the Soave-Redlich-Kwong equation of state, Fluid Phase Equilib., 143 (1998) 29-39.
[55] B.I. Lee, M.G. Kesler, A generalized thermodynamic correlation based on three-parameter corresponding states, AIChE J., 21 (1975) 510-527.
[56] M.G. Kesler, B.I. Lee, Improve prediction of enthalpy of fractions, Hydrocarbon. Process, 55 (1976) 153-158.
[57] T. Regueira, M.-L. Glykioti, N. Kottaki, E.H. Stenby, W. Yan, Density, compressibility and phase equilibrium of high pressure-high temperature reservoir fluids up to 473 K and 140 MPa, J. Supercrit. Fluids, 159 (2020) 104781.